Giant resonances in ^{116}Sn from 240 MeV ^{6}Li scattering

X. Chen, Y.-W. Lui, H. L. Clark, Y. Tokimoto, and D. H. Youngblood

Cyclotron Institute, Texas A&M University, College Station, Texas 77843, USA

Giant resonances in ^{116}Sn were measured by inelastic scattering of ^{6}Li ions at $E_{^6\text{Li}} = 240$ MeV over the angle range $0°$–$6°$. Isoscalar $E0$–$E3$ strength distributions were obtained with a double folding model analysis. A total of $106^{+27}_{-11}\%$ of the $E0$ EWSR was found in the excitation energy range from 8 MeV to 30 MeV with a centroid (m_1/m_0) energy $15.39^{+0.35}_{-0.20}$ MeV in agreement with results obtained with α inelastic scattering.

I. INTRODUCTION

Inelastic α particle scattering above $E_\alpha = 100$ MeV has been a valuable technique for studying isoscalar giant resonances for many years, and has been particularly successful for obtaining isoscalar monopole strength distributions [1,2] which are important for determining the compressibility of nuclear matter [3,4]. More recently, using beams of 240 MeV [5] and 400 MeV [6] α particles, the peak cross sections for the monopole resonance have been shown to approach 0.5 b/sr, sufficient to observe these resonances with low intensity rare isotope beams in inverse reactions. Unfortunately helium does not make a good target. At Riken a liquid He target $\sim$120 mg/cm^2 thick was developed and used to study the ISGMR in ^{14}O [7] with 60 MeV/nucleon^{14}O ions, however the energy straggling in such a target is large, and for heavier mass projectiles would be unacceptably large. The excitation of the GMR in the unstable nucleus ^{56}Ni has also been reported [8] using deuterium in the active target MAYA at Ganil [9].

A comparison of ISGMR energies with fully consistent HF-RPA calculations using Skyme interactions [10], gives a value of compressibility $K_{nm} = 230$–240 MeV, while a fully consistent relativistic random phase approximation (RRPA) [11], based on effective mean field Lagrangians with nonlinear meson self-interaction terms, points to a value of $K_{nm} = 250$–270 MeV, which is $\sim$12% higher. Piekarewicz [12] and Shlomo *et al.* [13–15] have shown that the difference in the values of K_{nm} obtained in the relativistic and non-relativistic models is mainly due to the differences in the values of symmetry energy coefficient J and its slope L associated with these models. In order to determine the contribution from symmetry energy accurately, a systematic study of ISGMR over a wide range of $(N\text{-}Z)/A$ is necessary. This range can be expanded by extending ISGMR measurements to unstable nuclei.

^{6}Li is also an isoscalar projectile ($N = Z$), and the inelastic scattering of ^{6}Li should preferentially excite isoscalar resonances as does α scattering [5]. Since solid targets of ^{6}Li in the few mg/cm^2 range are relatively easy to make, inelastic ^{6}Li scattering could be a particularly attractive way to study the isoscalar giant monopole (ISGMR) in unstable isotopes. The low particle emitting threshold for ^{6}Li gives a large breakup probability into the dominant channel ^{6}Li $\rightarrow \alpha + d$. Therefore the physical background due to multistep processes should be low for ^{6}Li scattering to the giant resonance energy range.

ISGMR studies in ^{12}C and ^{24}Mg with 156 MeV ^{6}Li inelastic scattering have been reported respectively by Eyrich *et al.* [16] and Dennert *et al.* [17] However, the low bombarding energy limited the useful excitation energy range to $E_x \leqslant 30$ MeV.

We report here studies of giant resonances in ^{116}Sn with inelastic ^{6}Li scattering at $E_{^6\text{Li}} = 240$ MeV detecting the ^{6}Li ions at small angles including $0°$ to enhance excitation of the ISGMR. The isoscalar giant resonances in ^{116}Sn have been studied in a number of works [2,5,18–21], mostly by inelastic α scattering, so this could provide both complementary information on the isoscalar resonances in ^{116}Sn and a test of the potential for using inelastic ^{6}Li scattering to study unstable nuclei. In a previous work [22], we reported optical model parameters (for both a Woods-Saxon potential and double folding models) obtained for 240 MeV ^{6}Li ions scattered from ^{116}Sn, where elastic scattering was used to obtain the parameters and it was shown that transition probabilities for low lying states obtained with double folding agreed with accepted values.

II. ENERGY WEIGHTED SUM RULES AND TRANSITION POTENTIALS

A. Energy weighted sum rule (EWSR) and transition density

The energy weighted sum rule (EWSR) is usually used as a measurement of the strength of isoscalar giant resonances. It is defined as a sum of the transition probabilities due to the excitation operator Q, from the ground state to all excited states multiplied, respectively, by the corresponding excitation energies [23]:

$$S(Q) \equiv \sum_n (E_n - E_0)|\langle n|Q|0\rangle|^2 = \frac{1}{2}\langle 0|[Q, [H, Q]]|0\rangle, \quad (1)$$

where n labels the complete set of excited states that can be reached by operating with Q on the ground state $|0\rangle$. For a multipole excitation operator

$$Q = \sum_i f(r_i) Y_L^M(\Omega_i), \quad (2)$$

the EWSR can be evaluated by means of the gradient formula and is obtained as [23]

$$S(Q) = \frac{2L+1}{4\pi} \frac{\hbar^2}{2m} A \left\langle \left(\frac{df}{dr}\right)^2 + L(L+1) \left(\frac{f}{r}\right)^2 \right\rangle, \quad (3)$$

where m is the mass of the nucleon and A is the mass number of the system.

With the isoscalar mass operator $Q_{0LM}(L \geqslant 2)$

$$Q_{0LM} = \sum_{i=1}^{A} r_i^L Y_L^M(\Omega_i), \quad (4)$$

the corresponding EWSR is obtained [24]

$$S(Q_{0LM}) = \frac{\hbar^2 A}{8\pi\,m} L(2L+1)^2 \langle r^{2L-2}\rangle, \quad (5)$$

where $\langle r^{2L-2}\rangle$ is the average over the ground state density distribution. The EWSR is independent of assumptions about nuclear structure.

The transition density ($L \geqslant 2$) can be obtained [24] using either Bohr-Mottelson (B-M) collective model or Tassie model. In the B-M collective model, a set of certain multipole deformation parameters is introduced to describe the deformed nucleus. Then, the density of the deformed nucleus is expressed in the Taylor expansion to the first order and is compared to its multipole expansion. Following the discussion in Ref. [24], the transition density for $L \geqslant 2$ can be expressed as

$$\rho_L(r) = -\beta_L R_0 \frac{d\rho(r)}{dr}, \quad L \geqslant 2, \quad (6)$$

where β_L is the deformation parameter. The square of the deformation length for a single state with excitation energy E_x which exhausts the EWSR can then be expressed as

$$\delta_L^2 = \beta_L^2 R_0^2 = \frac{2\pi\hbar^2}{m\,A\,E_x} \frac{L(2L+1)^2}{(L+2)^2} \frac{\langle r^{2L-2}\rangle}{\langle r^{L-1}\rangle^2}. \quad (7)$$

For an $L = 0$ (monopole) transition, the mass operator is given by

$$Q_{000} = \sum_{i=1}^{A} r_i^2 Y_{00} \quad (8)$$

and the corresponding EWSR is obtained by inserting the above expression into Eq. (3)

$$S_{EW}^{00} = \frac{A\hbar^2}{2\pi m} \langle r^2\rangle, \quad (9)$$

where m is the nucleon mass and $\langle r^2\rangle$ is averaged over the ground state density [24].

The transition density for a monopole resonance can be obtained with a simple scaling on radius [24,25]

$$\rho_0(r) \approx -\alpha_0 \left[3\rho(r) + r\frac{d\rho(r)}{dr}\right]. \quad (10)$$

If the excitation of a single state with excitation energy E_x exhausts the EWSR, the sum rule limit dimensionless

amplitude α_0 is obtained following the same procedure as for $L \geqslant 2$:

$$\alpha_0^2 = \frac{2\pi\hbar^2}{mAE_x\langle r^2\rangle}. \quad (11)$$

The collective formalism to describe isoscalar dipole excitations in electron scattering was first proposed by Deal *et al.* [26], and later extended to those excited with hadron scattering by Harakeh and Dieperink [27]. Following the discussion given by Harakeh and Dieperink, the EWSR for isoscalar dipole excitation can be obtained as [27]

$$S_{EW}^{01} = \frac{\hbar^2 A}{32m\pi} \left(11\langle r^4\rangle - \frac{25}{3}\langle r^2\rangle^2 - 10\varepsilon\langle r^2\rangle\right), \quad (12a)$$

where

$$\varepsilon = \frac{\hbar^2}{3mA} \left(\frac{4}{E_2} + \frac{5}{E_0}\right), \quad (12b)$$

where E_0 is the excitation energy of the ISGMR and E_2 is the excitation energy of the isoscalar quadruple resonance. Assuming the isoscalar dipole EWSR is exhausted by one state, the transition density of this state is [27]

$$g_1(r) = -\frac{\beta_1}{c\sqrt{3}} \left[3r^2 \frac{d}{dr} + 10r - \frac{5}{3}\langle r^2\rangle \frac{d}{dr} + \varepsilon \left(r\frac{d^2}{dr^2} + 4\frac{d}{dr}\right)\right] \rho(r) \quad (13a)$$

where

$$\beta_1^2 = \frac{6\pi\,\hbar^2}{m\,A\,E_x} \frac{c^2}{11\langle r^4\rangle - \frac{25}{3}\langle r^2\rangle^2 - 10\varepsilon\langle r^2\rangle} \quad (13b)$$

and β_1 is the collective coupling parameter and c is the half density radius of the Fermi mass distribution. The transition density given above (13a) is only for one of the magnetic substates and must be multiplied by $(2l+1)^{1/2}$ to represent excitation of the ISGDR [28].

B. Folding model transition potential

Following the formalism of the generalized folding model using the realistic density dependent M3Y-Paris nucleon-nucleon interaction described in Ref. [29], for a single excitation of the target nucleus **A**, the corresponding nuclear matrix element can be expressed as

$$\langle \alpha'(aA')|V|\alpha(aA)\rangle$$
$$= \sum_{\lambda\mu} C_\lambda \langle J_A M_A \lambda\mu | J_{A'} M_{A'}\rangle V_\lambda(E_\alpha, R)[i^\lambda Y_{\lambda\mu}(\hat{\tilde{R}})]^*, \quad (14)$$

where $\boldsymbol{\alpha}$ means incident scattering channel, α' means inelastic scattering channel, $\boldsymbol{a}$ means ground state of projectile and A' means single excitation of the target nucleus and

$$V_\lambda(E_\alpha, R) = V_\lambda^{(D)}(E_a, R) + V_\lambda^{(EX)}(E_\alpha, R), \quad (15)$$

where $V_\lambda^{(D)}(E_\alpha, R)$ and $V_\lambda^{(EX)}(E_\alpha, R)$ are direct term and exchange term, respectively. The details of discussion about $V_\lambda^{(D)}(E_\alpha, R)$ and $V_\lambda^{(EX)}(E_\alpha, R)$ are given in Ref. [29].

To evaluate the transition potential, there are two different methods to include the medium correction when a density dependent NN interaction is used [29,30]: (i) static treatment of the density dependence (SDD) in which only the ground state densities are included in the folding procedure, i.e.,

$$v_{D(EX)}(\rho, s) = F(\rho_0^a + \rho_0^A)v_{D(EX)}(s); \tag{16}$$

(ii) dynamic treatment of the density dependence (CDD) in which the effect of density changing due to the excitation is also included, i.e.,

$$\hat{v}_{D(EX)} = \left[F(\rho_0^a + \rho_0^A) + \frac{\partial F(\rho_0^a + \rho_0^A)}{\partial \rho_0^A} \rho_0^A \right] v_{D(EX)}(s). \tag{17}$$

However, according to Farid and Satchler [30], the difference between the two options resulted in 20% or less difference in peak cross sections in the case of α scattering to small angles, particularly relevant to giant resonance studies. The static treatment was used in this work.

III. DATA ANALYSIS

The inelastic scattering of ^{6}Li from ^{116}Sn over the excitation energy range 8 to 30 MeV was measured at spectrometer angles 0° and 4°. The experimental technique is similar to that described in Ref. [31] and is briefly summarized below. A beam of 240 MeV ^{6}Li particles from the Texas A&M University K500 superconducting cyclotron passed through a beam analysis system [32] and bombarded a self-supporting 9.9 mg/cm^2 Sn foil which was enriched to 95% in ^{116}Sn and located in the target chamber of the multipole-dipole-multipole spectrometer (MDM) [33]. The horizontal acceptance of the spectrometer was 4° and ray tracing was used to reconstruct the scattering angle. The vertical acceptance was ±2°. The outgoing particles were detected by a 60 cm long focal plane detector. The principles of operation of the detector are similar to the detector described in Ref. [34]. It contains four resistive wire proportional counters to measure position, as well as an ionization chamber to provide ΔE and a scintillator behind the ionization chamber to measure the energy deposited and provide a fast timing signal for each event. The out-of-plane scattering angle was not measured. The details of angle and position calibrations were described in Ref. [35]. Position resolution of approximately 0.9 mm and scattering angle resolution of about 0.09° were obtained. The energy calibration for inelastic scattering to the giant resonance region was obtained by measuring inelastic scattering from ^{12}C, ^{24}Mg, and ^{28}Si with the spectrometer set at 4°, at the actual field settings used in the experiments. The positions of the 3$^-$ state at $E_x = 10.18 \pm 0.02$ MeV and 2$^+$ states with $E_x = 18.67 \pm 0.05$, 20.43 ± 0.05 MeV [36] in ^{28}Si, the 2$^+$ state with $E_x = 17.36 \pm 0.05$ MeV [36] and 3$^-$ states with $E_x = 12.88 \pm 0.05$ in ^{24}Mg and $E_x = 9.641 \pm 0.005$, 18.35 ± 0.05 MeV [37] in ^{12}C were used for calibration. During the experiment, calibration runs with a ^{24}Mg target were done before and after the data runs to check the energy calibration at 0° using the 13.85 ± 0.05 MeV 0$^+$ state [36].
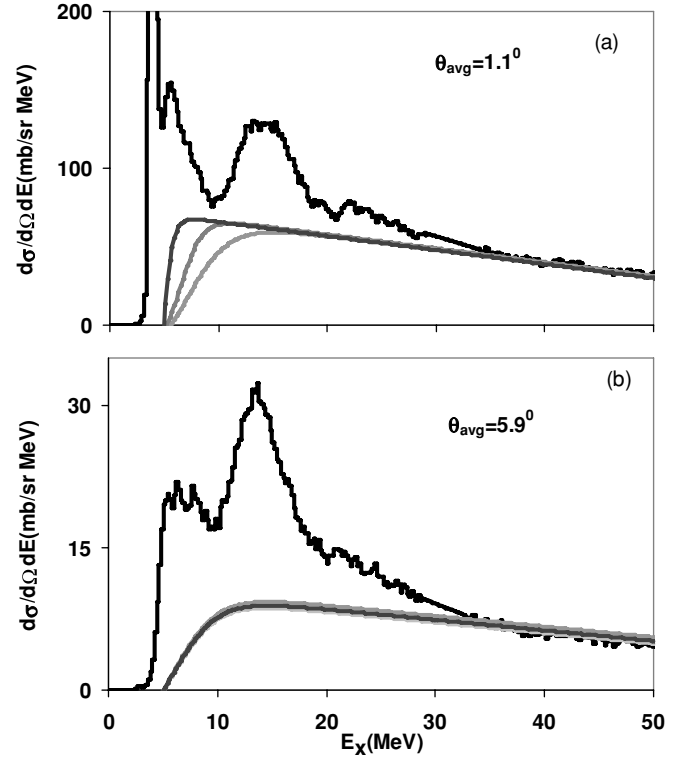

FIG. 1. Sample excitation spectra taken for average center of mass angles 1.1° and 5.9° for 240 MeV ^{6}Li ions scattered from ^{116}Sn. The gray curves represent different continuum choices used in the analysis.

Sample excitation energy spectra taken for average center of mass angles 1.1° and 5.9° are shown in Fig. 1. The excitation energy spectrum for each angle bin was divided into a peak and continuum. The continuum [18] may come from different physics processes such as multistep excitation of target, quasielastic scattering from target nucleons or nucleons clusters and excitations of noncollective states. However it is very difficult to quantitatively estimate the continuum, so an empirical procedure was used. The continuum was assumed to have the shape of a straight line at high excitation joining onto a Fermi shape at low excitation energy to model particle threshold effects as shown in Eq. (18) [35]:

$$Y = A + BE_X + \frac{Y_0}{1 + e^{\frac{E_x - E_{th}}{C}}}, \tag{18}$$

where A and B are determined from a fit to the high excitation region, E_{th} and C are adjusted to model the behavior of the spectrum near the particle threshold, and Y_0 is adjusted so that the continuum obtained is zero just below the particle threshold (6–7 MeV). Continua obtained in this way are illustrated by the solid gray lines on the spectra in Fig. 1.

A multipole decomposition technique [31,38,39] was used in the data analysis. The excitation energy range was divided into energy bins with widths each less than 2 MeV. The angular distributions of the differential cross sections for the peak and continuum were obtained for each energy bin and compared to distorted wave Born approximation (DWBA) calculations for isoscalar $E0$–$E4$ transitions. Several analyses were carried
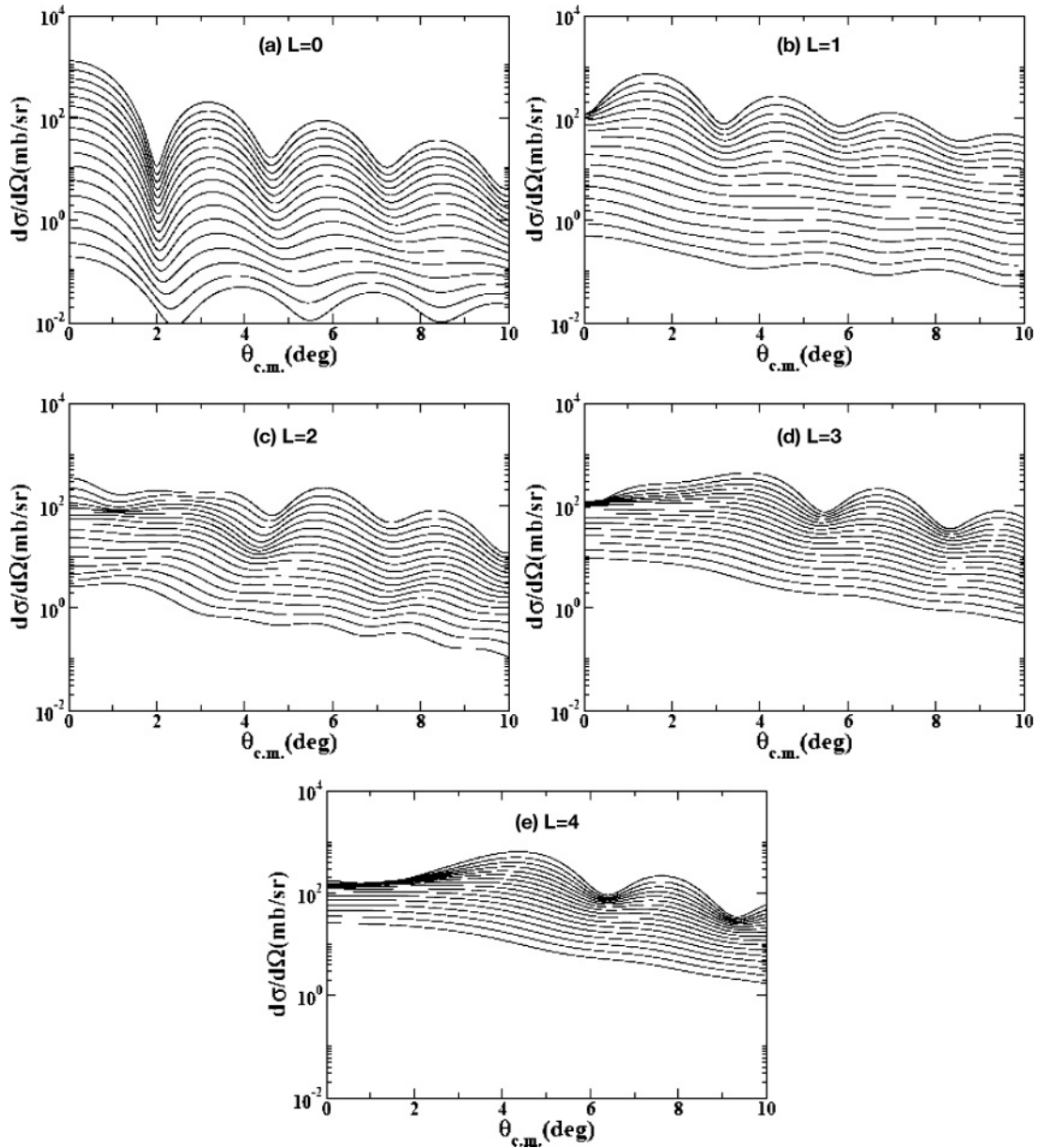
FIG. 2. Angular distributions of the differential cross sections for 240 MeV ^{6}Li inelastic scattering from ^{116}Sn for 100% of the respective EWSR for $L = 0$–4 over the excitation energy range 8–40 MeV in 2 MeV intervals. The cross sections decrease as the excitation energy increases.

out with different continua where the slope, intercept and cutoff were varied to reflect a variety of reasonable continuum choices [18]. The variety of continuum choices used in the analysis is illustrated in Fig. 1.

The DWBA calculations were done using the double folding model and the folded potential obtained with the DDF model (Table II of Ref. [22]). The transition potentials for $L = 0$–4 transitions were calculated with DFPD4 [40] for the excitation range from 8–40 MeV in 1 MeV steps. The angular distributions of the differential cross section for excitations exhausting 100% of the respective EWSR's were obtained with ECIS [41] over this same energy range and are shown in Fig. 2. The angular distributions for the different multipolarties ($L = 0$–4) for $E_x = 15.0$ MeV are compared

in Fig. 3. The angular distribution for $L = 0$ peaks at $0°$ and is well distinguished from the others. A set of sample angular distributions for 1.6 MeV wide bins centered at $E_x = 12.62, 22.20, 30.17$ MeV for the giant resonance peak and the continuum are shown in Fig. 4 along with DWBA fits. The isovector $E1$ (IVGDR) contributions were calculated from the known distributions [42] and were fixed in the fits.

The strength distributions obtained for isoscalar $E0$–$E3$ excitations of ^{116}Sn are plotted as black curves with Gaussian fits plotted in gray dot curves in Fig. 5. The GR strength distributions presented are the result of an average of the distributions obtained with different continua and the error bars shown on the multipole strength distributions were estimated by adding (in quadrature) the uncertainty from a multipole fit

TABLE I. Parameters obtained for $E0$, $E2$, $E3$ multipole distributions in ^{116}Sn in this work compared to those obtained from α scattering.

	240 MeV ^{6}Li scattering					α scattering			
	m_1/m_0 (MeV)	Γ^{*a} (MeV)	Centroid Gaussian fit (MeV)	Γ (MeV)	EWSR (%)	Ref.	m_1/m_0 (MeV)	Γ^* (MeV)[a]	EWSR (%)
$E0$	$15.39^{+0.35}_{-0.20}$	$6.10^{+0.85}_{-0.34}$	15.58 ± 0.19	5.46 ± 0.18	106^{+27}_{-11}	[18]	15.85 ± 0.20	5.27 ± 0.25	112 ± 15
						[19]	$15.9 \pm 0.5^*$		117 ± 12
						[21]	15.80 ± 0.10	4.10 ± 0.38	
$E2$	$14.34^{+0.26}_{-0.20}$	$6.90^{+0.78}_{-0.18}$	14.09 ± 0.27	5.48 ± 0.35	94^{+14}_{-10}	[18]	13.50 ± 0.35	5.0 ± 0.30	108 ± 12
						[19]	$14 \pm 0.5^*$		103 ± 10
$E3$	21.66 ± 0.21	10.87 ± 0.23			116 ± 11	[18]	23.3 ± 0.8	10.9 ± 0.6	70 ± 12
						[19]	21.8 ± 0.5	7.1 ± 0.5	67 ± 10

[a]Γ^* is the width (equivalent to FWMH for a Gaussian distribution) obtained by multiplying the rms width by 2.348 (see text).

to the standard deviations of all the fits obtained with different continuum choices.

The strength distributions obtained with α inelastic scattering [18] are plotted as gray curves in Fig. 5. The parameters obtained for $E0$, $E2$, and $E3$ excitations are given in Table I and those for $E1$ excitation are given in Table II and all are compared to those from Refs. [18,19]. There are two centroid energies listed in Table I. Following the notation in Ref. [18], the first one is m_1/m_0 and the second one is the peak position of Gaussian fit. Γ is the full width at half maximum (FWHM) for the Gaussian fit, while Γ^* is an equivalent FWHM obtained by multiplying the rms width by a factor of 2.3548

$$\text{rms width} = \sqrt{\frac{\sum_{i=1}^{n}(E_i - E_c)^2 S(E_i)}{\sum_{i=1}^{n} S(E_i)}}, \qquad (19)$$

where E_c is the centroid energy, E_i is the average energy of each energy bin and $S(E_i)$ is the corresponding strength for each bin.

The uncertainties for the centroid energy and rms width listed in Table I were calculated considering the uncertainty sources shown in Table III. An error in beam energy contributes very little to the uncertainty in excitation energy as a 5 MeV difference in beam energy gives a 0.004 MeV difference in excitation energy. The standard deviation from the fits to states used to do energy calibration contributes ~0.06 MeV of uncertainty. The uncertainty from the energy calibration slope, obtained by varying the minimum χ^2 by unit 1, varies with the excitation energy. The energy uncertainty of the 0^+ state of ^{24}Mg, which is used to adjust the energy calibration for the $0°$ spectra, is 0.06 MeV. The target thickness uncertainty gives about ~0.04 MeV energy uncertainty. All the above energy uncertainties are related to the energy calibration,

which affects the centroid but not the width. Using different widths for energy bins causes some changes in centroid energy and widths, estimated to contribute ~0.1 MeV to uncertainty in centroid. The systematic uncertainties, combined with the statistical fitting uncertainty, give the total uncertainty for each centroid energy and rms width.

The isoscalar $E0$ strength distribution obtained in this work corresponds to 106^{+27}_{-11}% of the $E0$ EWSR with $m_1/m_0 = 15.39^{+0.35}_{-0.20}$ MeV and $\Gamma^* = 6.10^{+0.85}_{-0.34}$ MeV. The energy and strength are in good agreement with those obtained with 240 MeV α scattering [18,19], and the width is somewhat larger, mostly due to small contributions at higher excitation. A Gaussian fit to the $E0$ strength distribution gives a centroid of 15.58 ± 0.19 MeV and a width of 5.46 ± 0.18 MeV. This width is in good agreement with the α scattering result. The centroid is also consistent with 15.80 ± 0.13 MeV given in Ref. [21] obtained with 400 MeV α inelastic scattering.

The isoscalar $E2$ strength extracted in this work corresponds to 94^{+14}_{-10}% of the $E2$ EWSR with a centroid of $14.34^{+0.26}_{-0.20}$ MeV and an equivalent width $6.90^{+0.78}_{-0.18}$ MeV. The energy is slightly higher than that reported more recently in 240 MeV α scattering [18], but within the errors of the earlier value reported for 240 MeV α scattering [19]. The strength obtained agrees well with that obtained with α scattering. The width is substantially larger than observed in α scattering. The Gaussian fit of the $E2$ strength distribution gives a centroid of 14.09 ± 0.27 MeV and a width of 5.48 ± 0.35 MeV. This width agrees with that found in α scattering, suggesting as for the $E0$ that small contributions fairly far from the centroid in the ^{6}Li data are contributing to the larger rms width in both cases.

The isoscalar $E3$ strength extracted in this work corresponds to 116 ± 11% of the $E3$ EWSR, which is much larger

TABLE II. ISGDR parameters for ^{116}Sn obtained from Gaussian fits compared to those obtained from α scattering.

	Peak1 centroid (MeV)	Γ (MeV)	EWSR (%)	Peak2 centroid (MeV)	Γ (MeV)	EWSR (%)	Total EWSR(%)
This work	15.32 ± 0.20	$5.56^{+0.20}_{-0.19}$	66 ± 10	21.73 ± 0.20	$2.80^{+0.26}_{-0.28}$	52^{+20}_{-14}	118^{+20}_{-14}
[18]	14.38 ± 0.25	5.84 ± 0.30	25 ± 15	25.5 ± 0.60	12.0 ± 0.6	61 ± 15	88 ± 20
[19]	14.7 ± 0.5	3.8 ± 1.2	13 ± 4	23.0 ± 0.6	8.7 ± 1.2	33 ± 11	46 ± 11

TABLE III. Contributions to energy uncertainty.

Uncertainty source	Energy uncertainty (MeV)
Beam energy uncertainty (± 5 MeV)	0.004
Calibration standard deviation	0.06
Calibration slope uncertainty	Varied with excitation energy
^{24}Mg(0^+, 13.86 MeV) uncertainty	0.06
Energy bin effect	0.1
Target thickness uncertainty	0.04
Statistical fitting uncertainty	Varied with centroid energy

than the $70 \pm 12\%$ identified in Ref. [18] and the $67 \pm 10\%$ extracted in Ref. [19]. The centroid energy obtained in this work agrees with that given in Ref. [19] while the width agrees with that given in Ref. [18].

The isoscalar $E1$ strength extracted in both ^{6}Li and α scattering is split into two peaks and the position of the lower peaks are similar, but otherwise there are significant differences. The $E1$ strength extracted in this work corresponds to $118^{+20}_{-14}\%$ of the $E1$ EWSR whereas 88% of the EWSR was identified with α scattering. The strength extracted from ^{6}Li scattering is larger but very little strength is seen above $E_x = 27$ MeV, while significant strength was seen with α scattering above 27 MeV. When fitted with two Gaussians, the low energy peak strength corresponds to $66 \pm 10\%$ of the $E1$ EWSR with a centroid of 15.32 ± 0.20 MeV and a width (FWHM) of $5.56^{+0.20}_{-0.19}$ MeV, the high energy peak strength corresponds to $52^{+20}_{-14}\%$ of the EWSR with a centroid energy of 21.73 ± 0.20 MeV and a width (FWHM) of $2.8^{+0.26}_{-0.28}$ MeV, while, in α scattering [18], the low energy peak corresponds to $25 \pm 15\%$ of the $E1$ EWSR
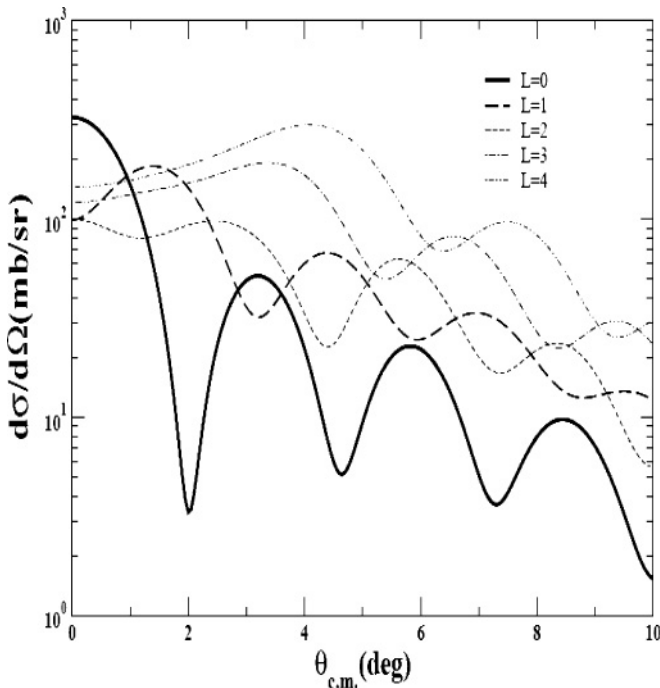

FIG. 3. Angular distributions of the differential cross section for 240 MeV ^{6}Li inelastic scattering from ^{116}Sn for $L = 0$–4 for 100% of the EWSR at $E_x = 15.0$ MeV.
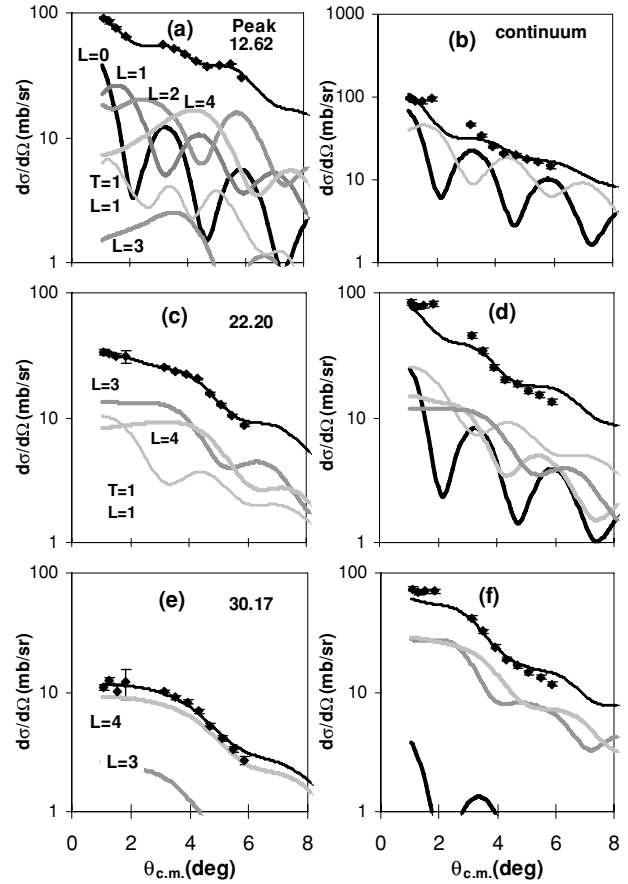

FIG. 4. Angular distributions of the cross section for inelastic scattering of 240 MeV ^{6}Li from ^{116}Sn for portions of the giant resonance peak and the continuum along with DWBA fits. The data are summed over 1.6 MeV wide excitation energy bins centered at $E_x =$ 12.62, 22.20, 30.17 MeV. The angular distributions for the giant resonance peak are on the left and those for the continuum are on the right. The thin black lines through the data show the fits. The $E0$ contribution is shown by the thick black line, with contributions from other multipoles labeled in the figure.

with a centroid of 14.38 ± 0.25 MeV and a width (FWHM) of 5.84 ± 0.30 MeV, the high energy peak corresponds to $61 \pm 15\%$ of the EWSR with a centroid energy of 25.50 ± 0.60 MeV and width (FWHM) of 12.0 ± 0.6 MeV. Youngblood *et al.* pointed out in a series of papers [18,43,44] that the $E1$ strength distributions are quite sensitive to continuum choices. The large difference in $E1$ strength shown here may be due at least in part to different continuum shapes in ^{6}Li and α scattering.

The ^{116}Sn giant resonance data were also analyzed with the deformed potential model. The distributions of the energy weighted sum rule (EWSR) strength obtained for isoscalar $E0$–$E3$ transitions of ^{116}Sn are shown in Fig. 6. The peak positions of the ISGMR and ISGQR strength distribution are consistent with those obtained from α inelastic scattering, but the strengths obtained from deformed potential analysis of ^{6}Li scattering were less than those obtained from a folding analysis of α scattering. No matter how the continuum was chosen, the strength of ISGDR obtained in the deformed potential analysis
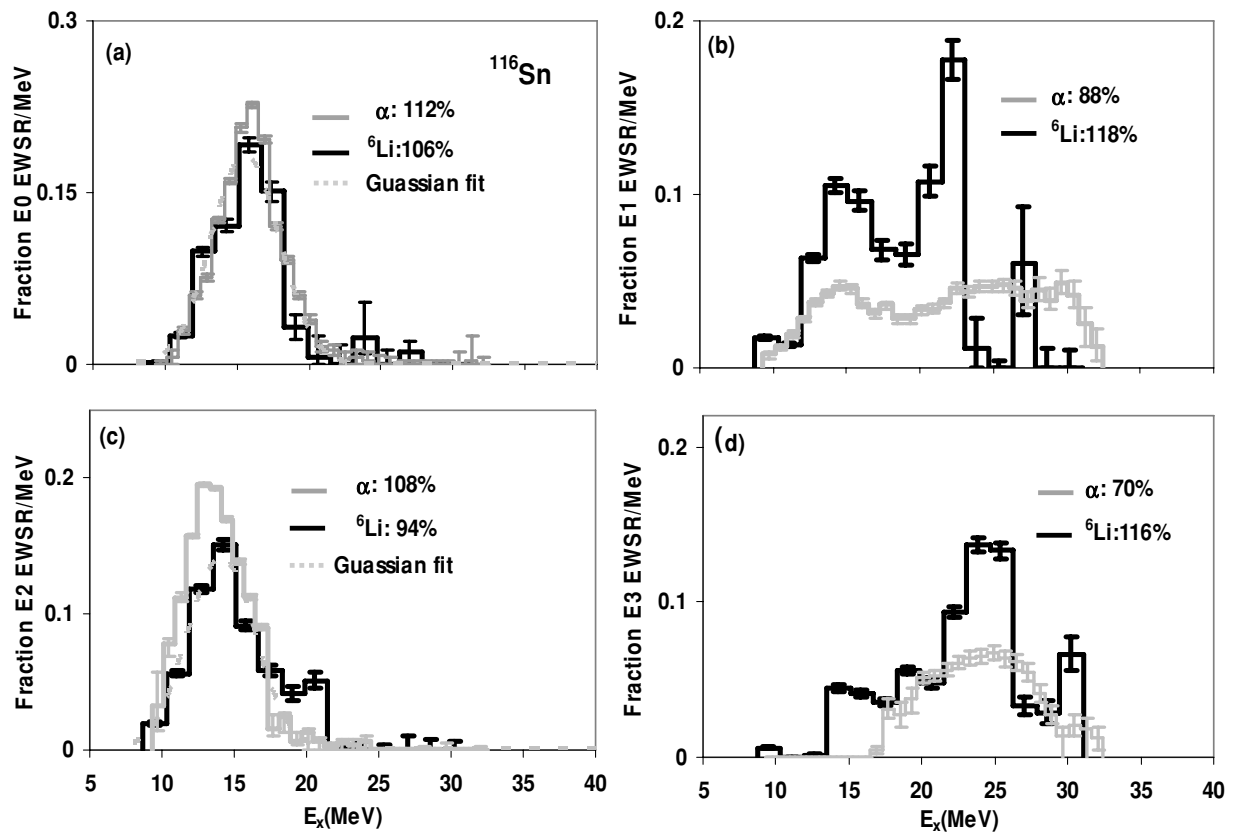
FIG. 5. Isoscalar $E0$–$E3$ EWSR Strength distributions (a: $E0$, b: $E1$, c: $E2$, d: $E3$) for ^{116}Sn obtained from analysis of ^{6}Li inelastic scattering (black). Those obtained with α inelastic scattering [18] are shown in gray. Error bars represent the uncertainty due to the fitting of the angular distributions and different choices of the continuum as described in the text.

was always much higher than 100% of the EWSR. Clark *et al.* [45] have pointed out that the predicted cross section for the ISGDR is very sensitive to the imaginary component of the optical and transition potential in α scattering when using the deformed potential model, and this may also be true for ^{6}Li scattering. The inability of the deformed potential model to reproduce transition strengths for other multipolarities has been well documented [46].
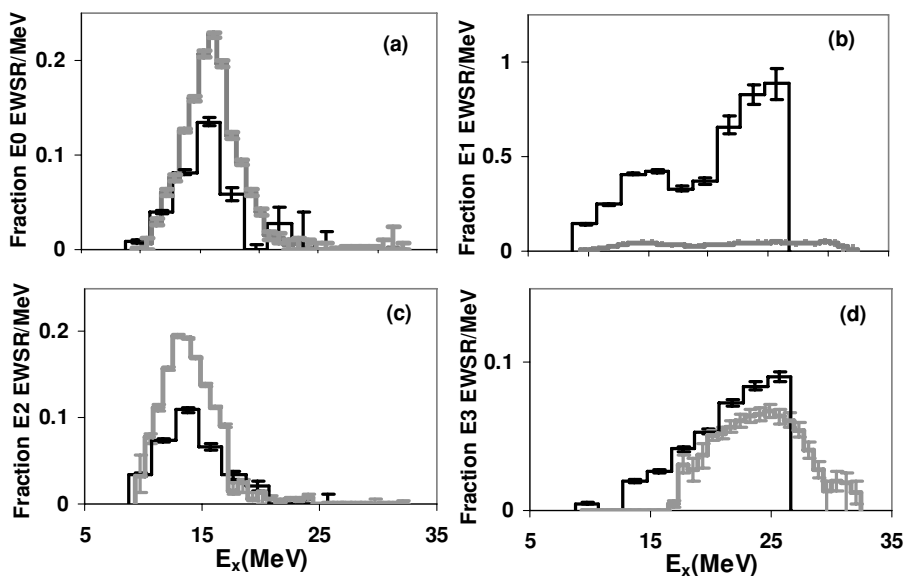

FIG. 6. Comparison of the strength distribution for $E0$–$E3$ transitions (a: $E0$, b: $E1$, c: $E2$, d: $E3$) extracted from ^{6}Li inelastic scattering using the deformed potential model (black) with those obtained from α inelastic scattering [37] using a folding potential (gray).

IV. SUMMARY AND CONCLUSIONS

Inelastic scattering of 240 MeV ^{6}Li ions exciting ^{116}Sn into the giant resonance region was analyzed with a density dependent folding (DDF) model and also with deformed potential model based on a Woods-Saxon phenomenological potential. The isoscalar $E0$ and $E2$ EWSR strength distributions of ^{116}Sn obtained with ^{6}Li scattering using the DDF model are mostly in agreement with those obtained from 240 MeV α scattering. The isoscalar $E1$ and $E3$ EWSR strength distributions obtained from ^{6}Li scattering differ substantially from those obtained with α scattering, indicating that the uncertainty in extracting these broad $E1$ and $E3$ strengths is considerably greater than that for the more concentrated $E0$ and $E2$ distributions. The strengths obtained in the deformed potential model analysis differ substantially from those obtained with folding analyses, which is a known issue [46]. The agreement between ^{6}Li and α scattering for the $E0$ resonance and the large cross section for excitation of the GMR in ^{6}Li scattering indicates that ^{6}Li inverse reactions could be a good tool to study the GMR in unstable nuclei.

[1] D. H. Youngblood, C. M. Rozsa, J. M. Moss, D. R Brown, and J. D. Bronson, Phys. Rev. Lett. **39**, 1188 (1977).

[2] D. H. Youngblood, P. Bogucki, J. D. Bronson, U. Garg, Y.-W. Lui, and C. M. Rozsa, Phys. Rev. C **23**, 1997 (1981).

[3] J. P. Blaizot, Phys. Rep. **64**, 171 (1980).

[4] S. Stringari, Phys. Lett. **B108**, 232 (1982).

[5] D. H. Youngblood, H. L. Clark, and Y.-W. Lui, Phys. Rev. Lett. **82**, 691 (1999).

[6] M. Uchida, H. Sakaguchi, M. Itoh *et al.*, Phys. Lett. **B557**, 12 (2003).

[7] H. Baba, S. Shimoura, T. Minemura *et al.*, Nucl. Phys. **A788**, 188 (2007).

[8] C. Monrozeau, E. Khan, Y. Blumenfeld *et al.*, Nucl. Phys. **A788**, 182 (2007).

[9] C. E. Demonchy, thesis T 03 06, Dec. 2003 (Université Caen, France, 2003).

[10] I. Hamamoto, H. Sagawa, and X. Z. Zhang, Phys. Rev. C **56**, 3121 (1997).

[11] Z.-Y. Ma, N. Van Giai, A. Wandelt *et al.*, Nucl. Phys. **A686**, 173 (2001).

[12] J. Piekarewicz, Phys. Rev. C **66**, 034305 (2002).

[13] S. Shlomo, V. Kolomietz, and G. Colò, Eur. Phys. J. A **30**, 23 (2006).

[14] S. Shlomo, B. K. Agrawal, and A. V. Kim, Nucl. Phys. **A734**, 589 (2004).

[15] B. K. Agrawal, S. Shlomo, and A. V. Kim, Phys. Rev. C **68**, 031304(R) (2003).

[16] W. Eyrich, A. Hofmann, A. Lehmann *et al.*, Phys. Rev. C **36**, 416 (1987).

[17] H. Dennert, E. Aschenauer, W. Eyrich *et al.*, Phys. Rev. C **52**, 3195 (1995).

[18] D. H. Youngblood, Y.-W. Lui, H. L. Clark, B. John, Y. Tokimoto, and X. Chen, Phys. Rev. C **69**, 034315 (2004).

[19] H. L. Clark, Y.-W. Lui, and D. H. Youngblood, Phys. Rev. C **63**, 031301(R) (2001).

[20] M. M. Sharma, W. T. A. Borghols, S. Brandenburg, S. Crona, A. vander Woude, and M. N. Harakeh, Phys. Rev. C **38**, 2562 (1988).

[21] U. Garg, T. Li, S. Okumura *et al.*, Nucl. Phys. **A788**, 36c (2007).

[22] X. Chen, Y.-W. Lui, H. L. Clark, Y. Tokimoto, and D. H. Youngblood, Phys. Rev. C **76**, 054606 (2007).

[23] A. Bohr and B. R. Mottleson, *Nuclear Structure II* (Benjamin, New York, 1975).

[24] G. R. Satchler, *Direct Nuclear Reactions* (Oxford University Press, New York, 1983).

[25] H. Uberall, *Electron Scattering from Complex Nuclei* (Academic Press, New York, 1971).

[26] T. J. Deal, Nucl. Phys. **A217**, 210 (1973).

[27] M. N. Harakeh and A. E. L. Dieperink, Phys. Rev. C **23**, 2329 (1981).

[28] D. H. Youngblood, Y.-W. Lui, and H. L. Clark, Phys. Rev. C **65**, 034302 (2002).

[29] D. T. Khoa and G. R. Satchler, Nucl. Phys. **A668**, 3 (2000).

[30] M. E.-A. Farid and G. R. Satchler, Nucl. Phys. **A481**, 542 (1988).

[31] D. H. Youngblood, Y.-W. Lui, and H. L. Clark, Phys. Rev. C **60**, 014304 (1999).

[32] D. H. Youngblood and J. D. Bronson, Nucl. Instrum. Methods Phys. Res. A **361**, 37 (1995).

[33] D. M. Pringle, W. N. Catford, J. S. Winfield *et al.*, Nucl. Instrum. Methods Phys. Res. A **245**, 230 (1986).

[34] D. H. Youngblood, Y.-W. Lui, H. L. Clark *et al.*, Nucl. Instrum. Methods Phys. Res. A **361**, 539 (1995).

[35] D. H. Youngblood, Y.-W. Lui, and H. L. Clark, Phys. Rev. C **55**, 2811 (1997).

[36] K. Van Der Borg, M. N. Harakeh, and A. Van Der Woude, Nucl. Phys. **A365**, 243 (1981).

[37] F. Ajzenberg-Selove, Nucl. Phys. **A506**, 1 (1990).

[38] D. H. Youngblood, Nucl. Phys. **A687**, 1c (2001).

[39] D. H. Youngblood, Y.-W. Lui, and H. L. Clark, Phys. Rev. C **63**, 067301 (2001).

[40] D. T. Khoa (unpublished, 2000).

[41] J. Raynal (unpublished).

[42] S. S. Dietrich and B. L. Berman, At. Data Nucl. Data Tables **38**, 199 (1988).

[43] D. H. Youngblood, Y.-W. Lui, B. John, Y. Tokimoto, H. L. Clark, and X. Chen, Phys. Rev. C **69**, 054312 (2004).

[44] D. H. Youngblood, Y.-W. Lui, and H. L. Clark, Phys. Rev. C **76**, 027304 (2007).

[45] H. L. Clark, Y.-W. Lui, and D. H. Youngblood, Nucl. Phys. **A687**, 80 (2001).

[46] J. R. Beene, D. J. Horen, and G. R. Satchler, Phys. Rev. C **48**, 3128 (1993).